Electronic Supplementary Material (ESI) for Journal of Materials Chemistry A.

Supporting information

Room-Temperature All-solid-state Lithium Metal Batteries Based on Ultrathin Polymeric Electrolytes

Jianwen Feng,[a] Jiayi Wang,[a] Qiao Gu,[a] Wadeelada Thitisomboon,[a] Dahua Yao,[b] Yonghong Deng,[b,*] Ping Gao[a,*]

[a] Advanced Materials Thrust, Function Hub and Department of Chemical and Biological Engineering, The Hong Kong University of Science and Technology, Clear Water Bay, Hong Kong, China.

[b] Department of Materials Science and Engineering, Southern University of Science and Technology, Shenzhen 518055, China.

[*] Corresponding authors:

E-mail: kepgao@ust.hk (P. Gao), dengyh@sustech.edu.cn (Y. Deng).

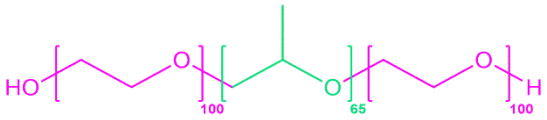

Figure S1. Chemical structure of Pluronic F127 copolymer. The green part represents the PPO blocks, while the purple part represents the PEO part.

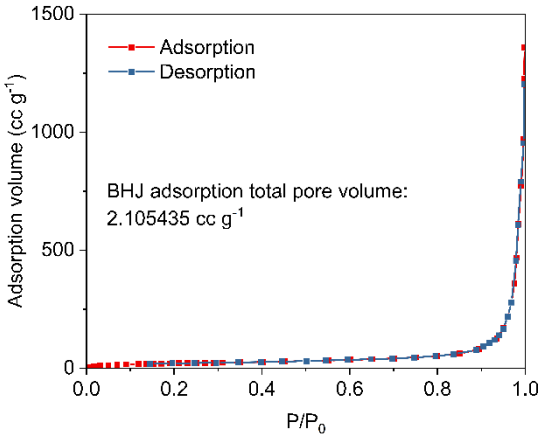

Figure S2. BET adsorption isotherms of PE membrane using nitrogen.

Assume that the density of bulk PE membrane is 0.96 g cm^{-3}. For 1 gram PE membrane, the solid PE takes up a volume of 1.04 cm^3. Then the porosity can be calculated by the formula below:

$$Porosity = \frac{2.105435}{(2.105435 + 1.04)} \times 100\% = 66.9\%$$

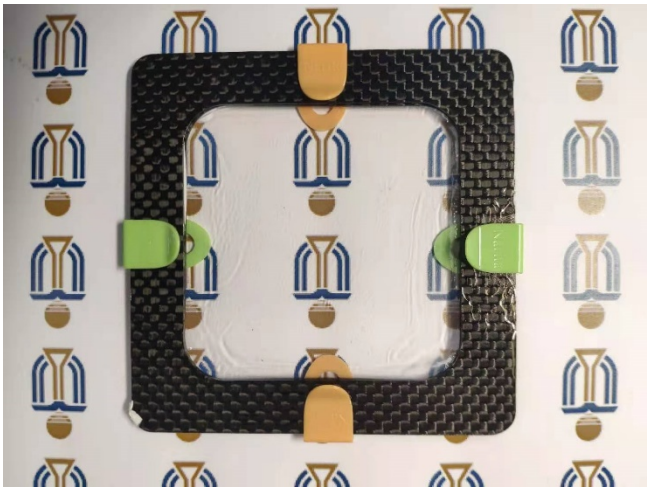

Figure S3. Image of prepared LTSPE.

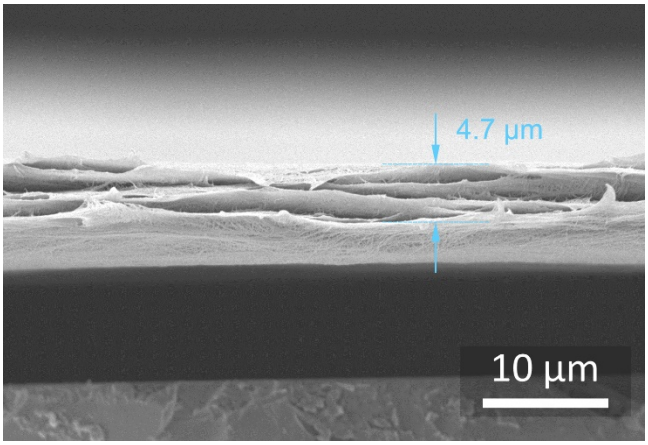

Figure S4. Cross-section SEM image of the ultrathin PE membrane.

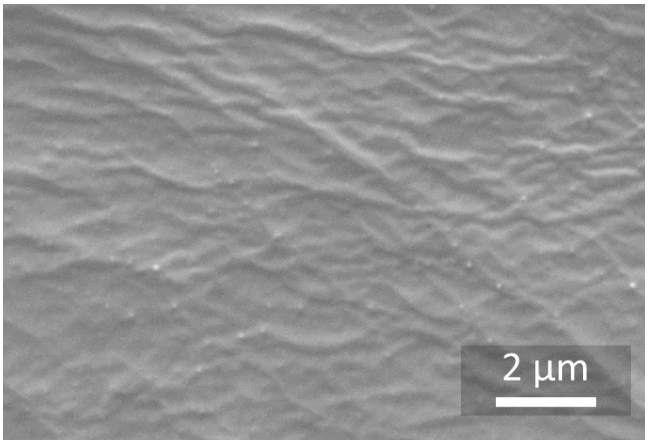

Figure S5. Top-view SEM images showing the surface morphology of the LTSPE membrane.

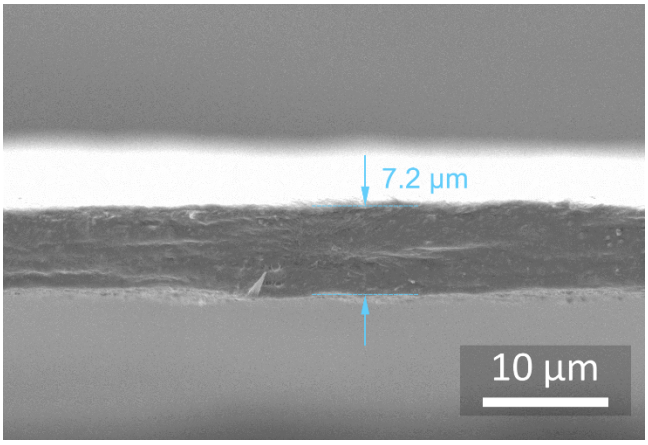

Figure S6. Cross-section SEM image of the LTSPE.

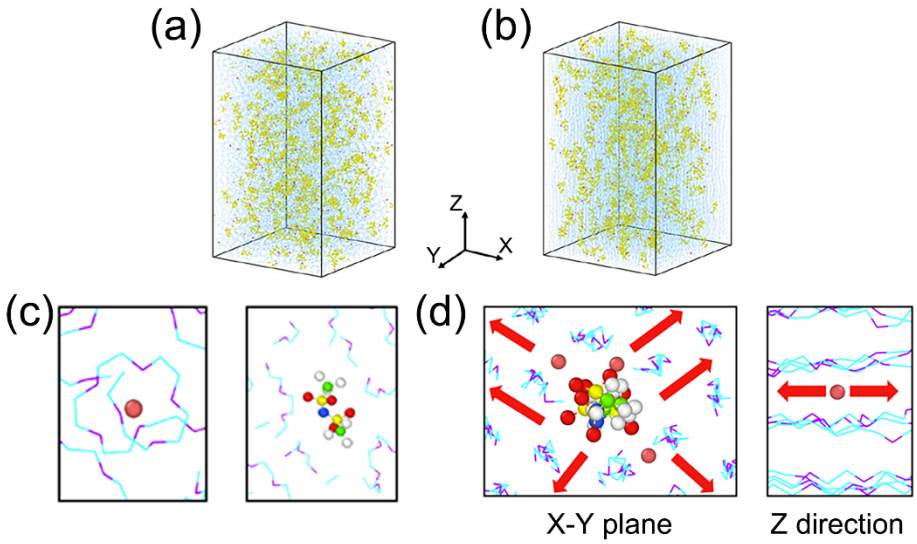

Figure S7. 3D view of PEO-LiTFSI simulation system in amorphous (a) and crystalline (b) state. Spatial configuration showing the interaction between ions and PEO chain in amorphous (c) and crystalline (d) state.

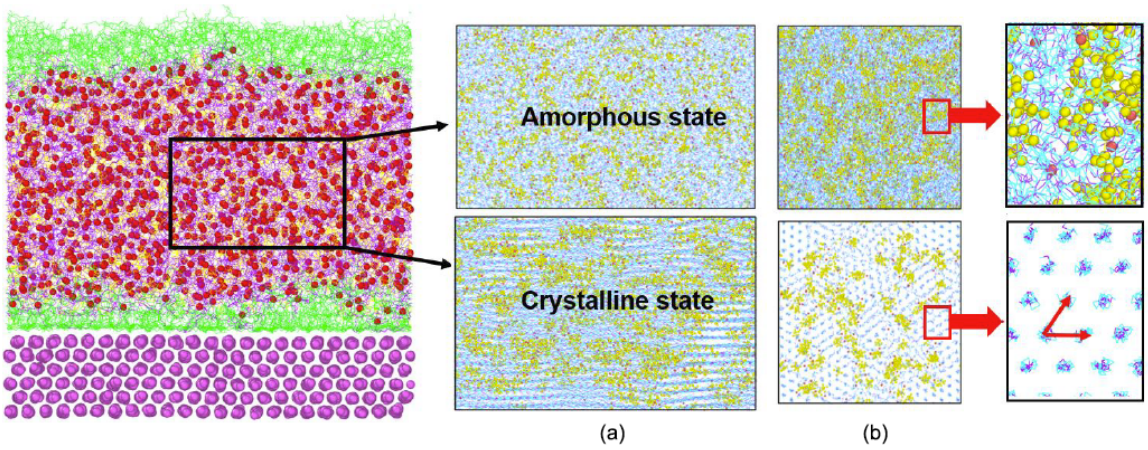

Figure S8. (a) Side view and (b) top view of the ion diffusion structure of the SPE in amorphous and crystalline state, respectively.

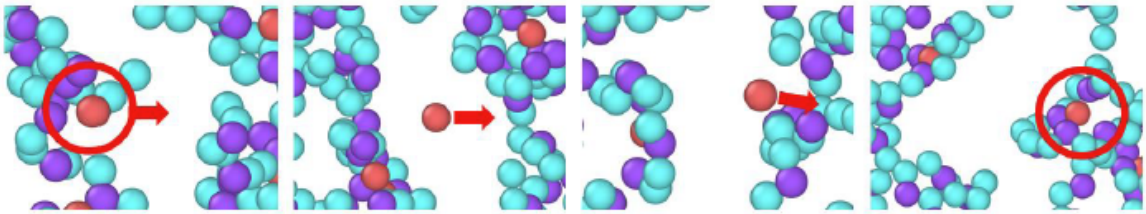

Figure S9. Diffusion progress of Li^+ in amorphous PEO. (a) Li^+ is entangled by a PEO chain. (b) Li^+ are released from a PEO chain. (c) Li^+ is attracted by a new PEO chain. (d) PEO chain forms a new entanglement to encircle Li^+.

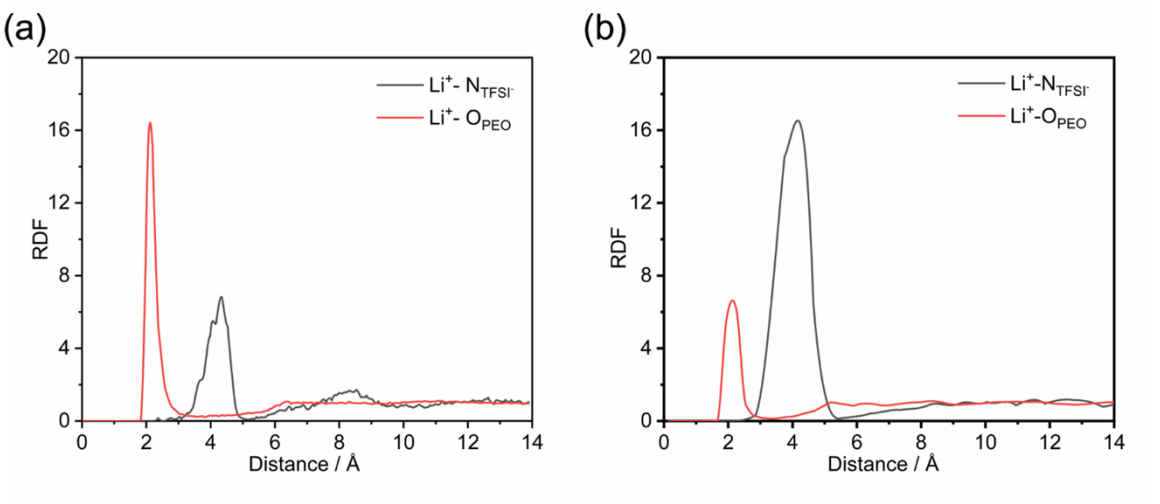

Figure S10. Coordination environment of Li^+ in (a) amorphous PEO region and (b) crystalline PEO region represented by radial distribution function (RDF).

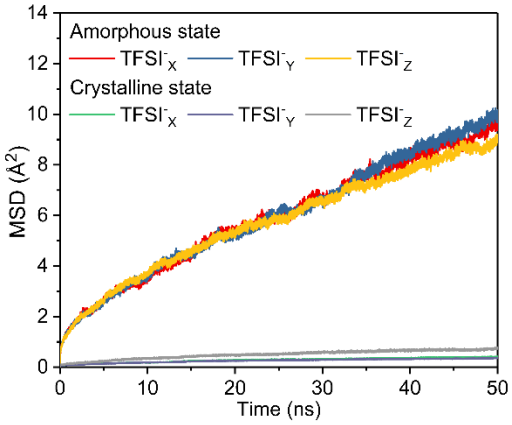

Figure S11. MSDs versus diffusion time of TFSI anions transport in crystalline and amorphous PEO system.

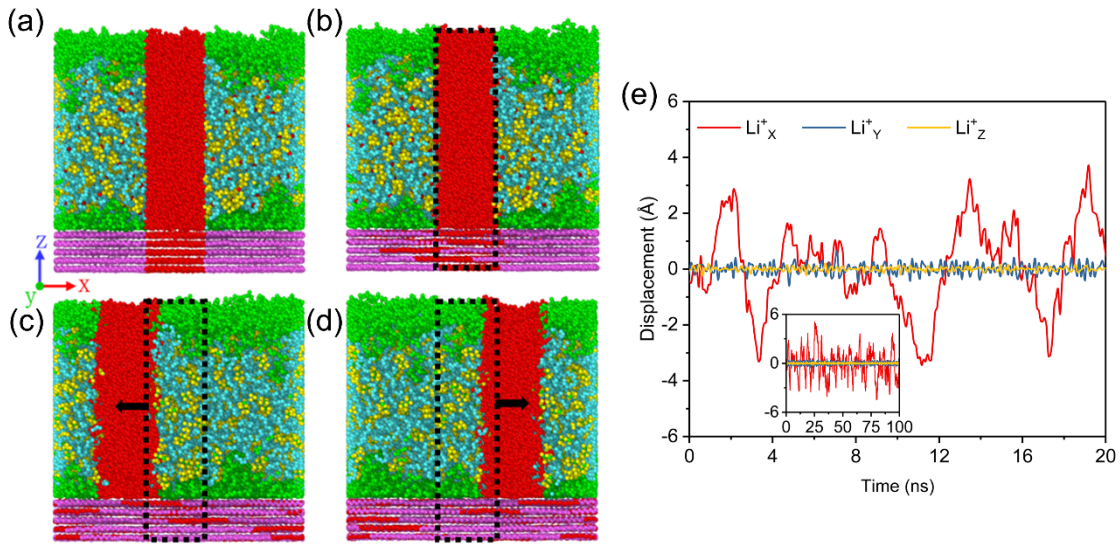

Figure S12. The slip process of the SPE (OL 12) on the PE fiber surface. (a) Before slip, all atoms in the middle of the system (including PE fiber) are marked in red so that the motion of PE and the SPE can be observed. (b) Simulation starts. The slip of PE fibers is not integral. (c) The SPE slides to the left as a whole. (d) The SPE slides to the right as a whole. (e) The displacement of Li+ along X, Y and Z directions in a time scale of 20 ns. The inset shows the displacement in a larger time scale (100 ns). The displacement is calculated every 50000-time steps.

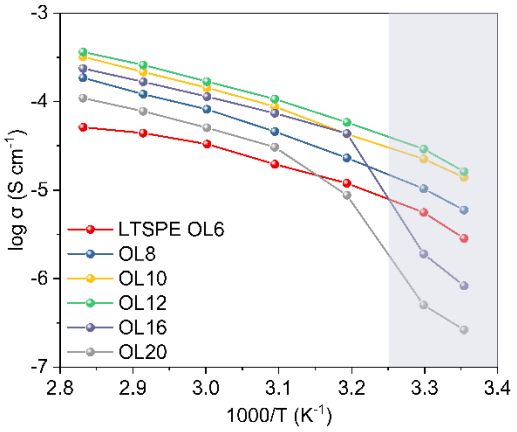

Figure S13. Ionic conductivity versus temperature curves of LTSPE with different OL ratio.

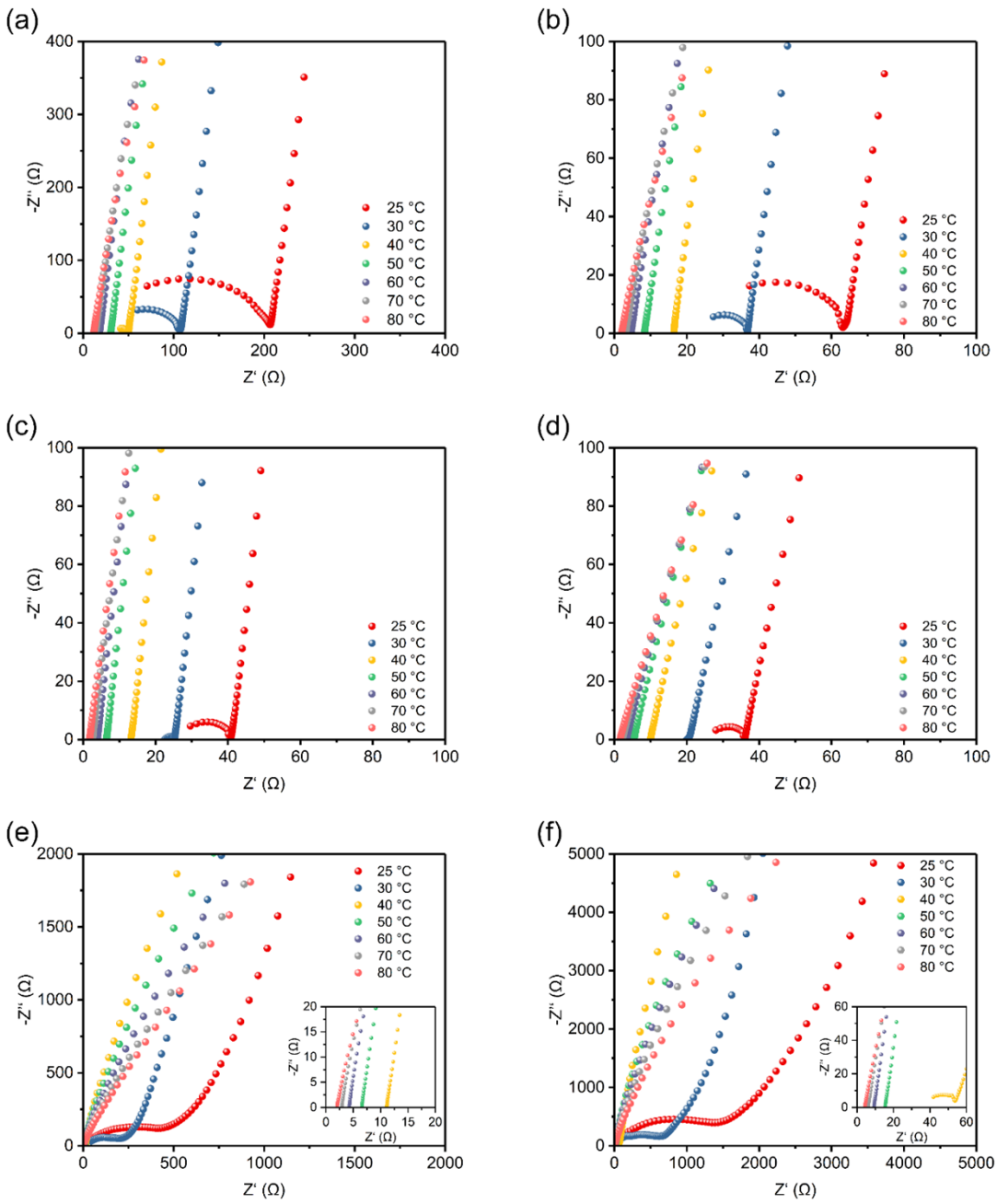

Figure S14. Nyquist plots of LTSPE with OL ratio of (a) 6, (b) 8, (c) 10, (d) 12, (e) 16 and (f) 20, respectively.

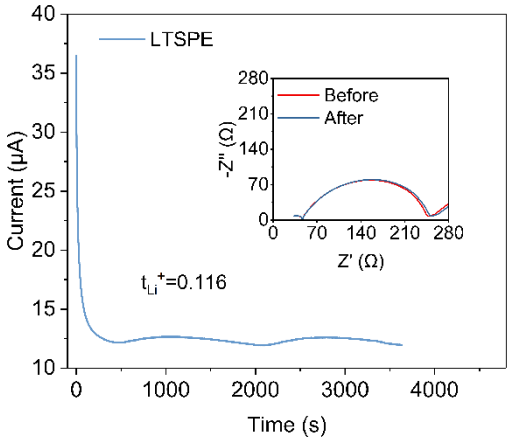

Figure S15. Transference number of the LTSPE (OL 12).

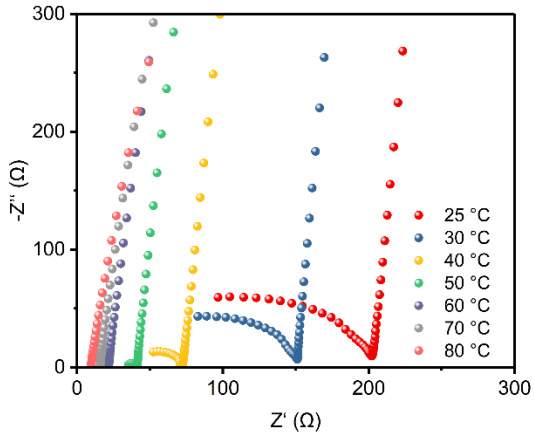

Figure S16. Nyquist plots of Celgard-F127-SPE with OL ratio of 12.

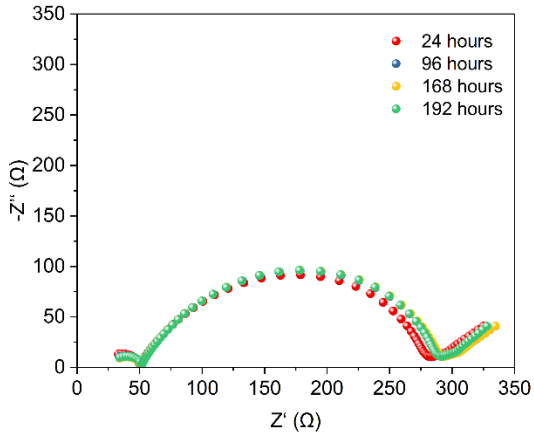

Figure S17. Nyquist plots of Li/LTSPE/Li symmetric cells after different storage time.

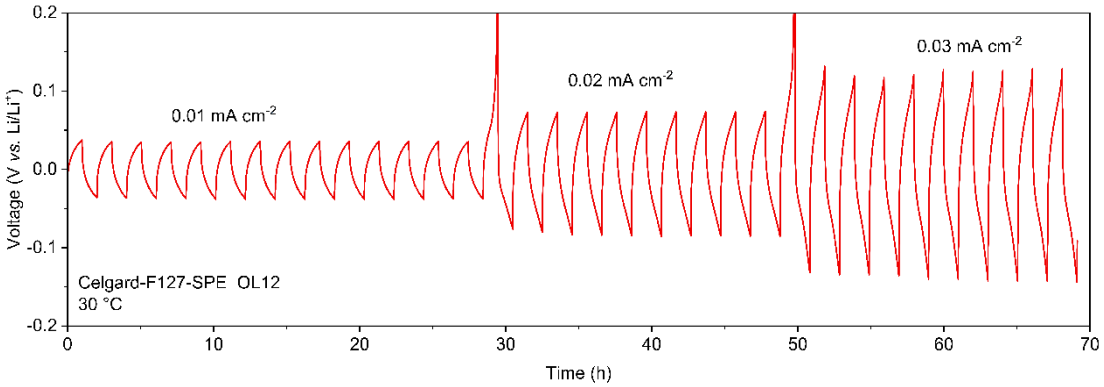

Figure S18. Cycling performance of Li/Celgard-F127-SPE/Li battery.

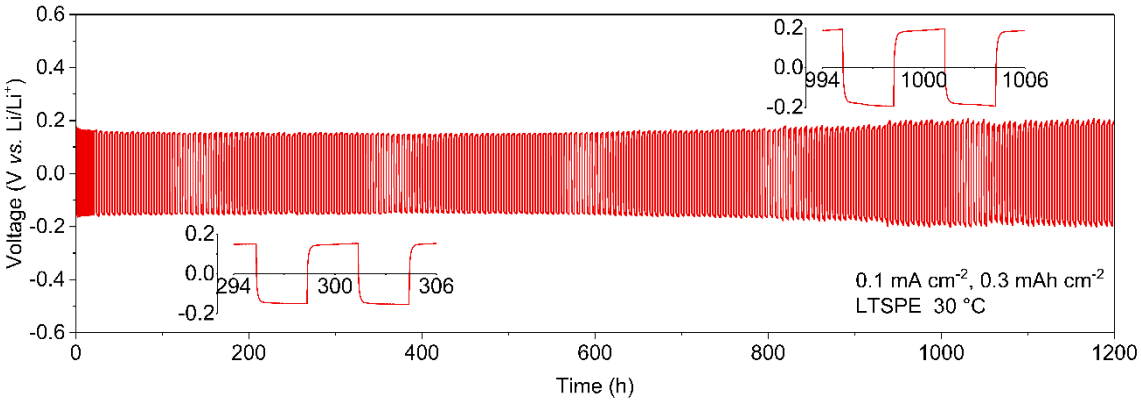

Figure S19. Cycling performance of Li/LTSPE/Li symmetric cells at a current density of 0.1 mA cm^{-2} with a capacity of 0.3 mAh cm^{-2} at 30 °C. The insets are voltage profiles of the corresponding symmetric batteries at 300 h and 1000 h, respectively.

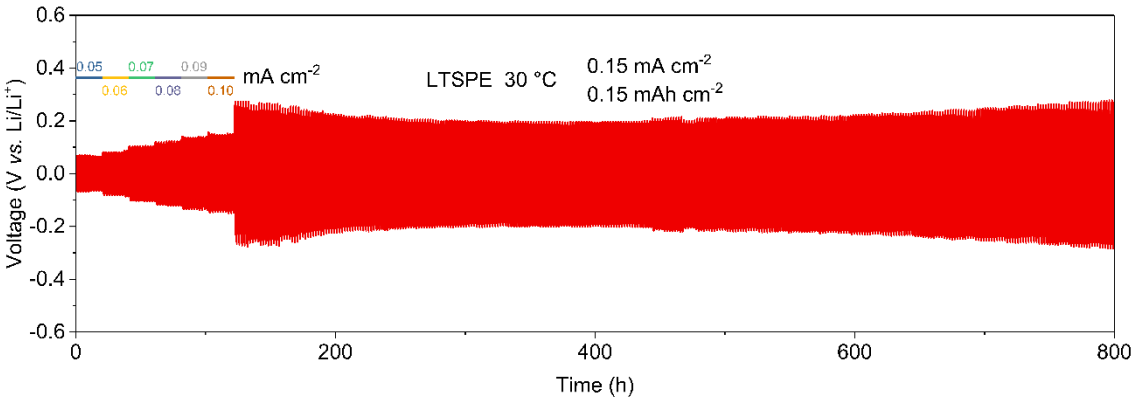

Figure S20. Cycling performance of Li/LTSPE/Li symmetric cells at a current density of 0.15 mA cm^{-2} with a capacity of 0.15 mAh cm^{-2} at 30 °C.

It is observed that the overpotential gradually decreases at first, which is because of the wetting process occurs during cycling. Therefore, the overpotential decrease with the wetting of the interface between Li metal and the PE-F127-SPE. Previous studies also show similar phenomenon.[1,2] As the cycling continue, the overpotential undergoes a certain level of increase. The overpotential increase here can be ascribed to the side reaction between terminal hydroxide group of PEO-PPO-PEO and Li metal under a high current density.[3]

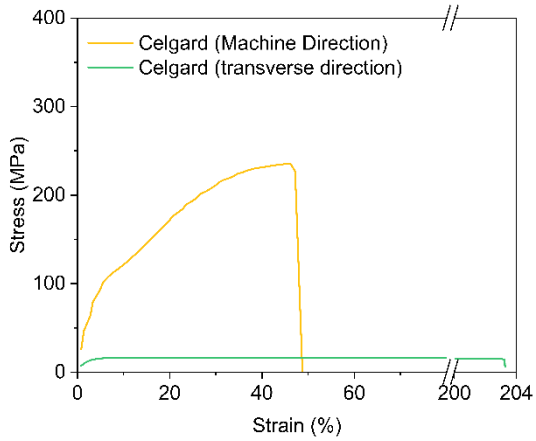

Figure S21. Stress-strain curves of the commercial Celgard 2500 membrane.

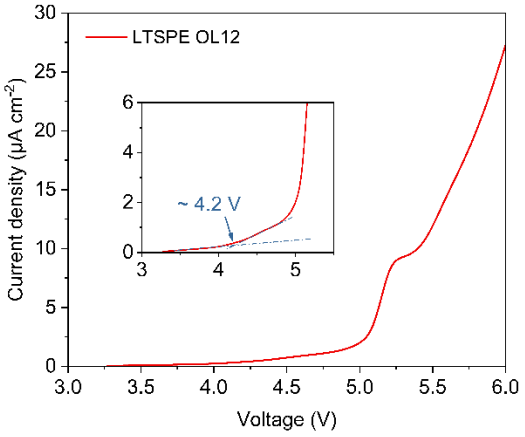

Figure S22. LSV curve of LTSPE with OL ratio of 12.

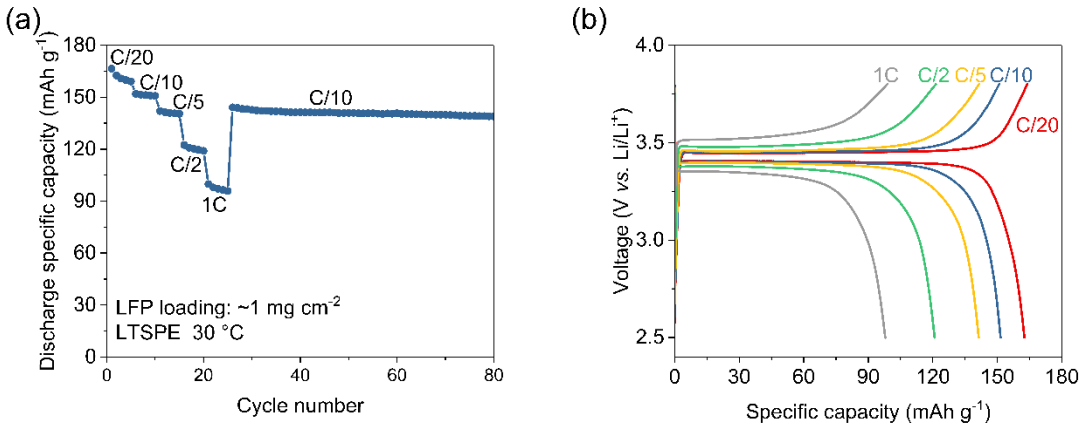

Figure S23. (a) Rate performance of Li/LTSPE/LFP battery at 30 °C. (b) Charge-discharge curves of Li/LTSPE/LFP battery at different rate.

Table S1. Summary of melting temperature and crystallinity of different samples.

Sample name	OL ratio	Melting temperature [°C]	Crystallinity [%]
LTSPE	6	/	/
	8	/	/
	10	/	/
	12	/	/
	16	36.4	35.38
	20	39.7	52.42
Pure F127	/	55.7	83.39

Table S2. Thickness of different samples for ionic conductivity calculation.

Sample name	OL ratio	Sample thickness [μm]
LTSPE	6	8
	8	5.1
	10	7.6
	12	7.8
	16	6.5
	20	6.3
Celgard-F127-SPE	12	25.2

After ionic conductivity measurement, the battery was disassembled. Then the thickness of SS/LTSPE/SS and SS/SS were measured respectively. The true thickness of SPE was obtained by subtracting the thickness of SS/SS from SS/LTSPE/SS.

Table S3. Parameters of tensile test samples and tensile strength results.

Sample name	Thickness [μm]	Width [mm]	Max normal force [N]	Tensile strength (Without porosity correction) [MPa]	Tensile strength (With porosity correction) [MPa]
PE membrane	4.7	5	3.30569	140.7	351.7
LTSPE	4.7	5	3.23234	137.5	343.9

Table S4. Comparison of Li-Li symmetric battery performance.

Sample name	Current density [mA cm^{-2}]	Lithium deposition time [h]	Stable cycling time [h]	Operation temperature [°C]	
PI/PEO/LiTFSI[4]	0.1	1	1000	60	PEO-based solid polymer electrolytes
	0.1	1	200	40	
PPL (PE-PEO-LiTFSI)[5]	0.1	1	1500	60	
PEO_8–LiPCSI[6]	0.01	1	1000	60	
PEO-LiTFSI-1 wt% $Mg(TFSI)_2$[7]	0.1	1	1700	50	
	0.2	0.5	>1400	50	
PEO/ZIF-90-g-IL[8]	0.1	1	700	60	PEO-based composite polymer electrolytes
PEO–$LiClO_4$–fumed SiO_2 (FS)[9]	0.02	1	380	60	
PEO-LiTFSI-5% MZ-CPE[10]	0.09	1	250	60	
PEO/LiTFSI/LiDGO[11]	0.1	1	1000	45	
PEO-LiTFSI/ZIF-8[12]	0.1	1	300	60	
PEO/LiTFSI/6% h-BN[13]	0.2	1	430	60	
Our work (LTSPE)	**0.1**	**1**	**3500**	**30**	
	0.15	**1**	**680**	**30**	
	0.1	**3**	**1200**	**30**	

References

1 S. Chen, J. Wang, Z. Wei, Z. Zhang, Y. Deng, X. Yao and X. Xu, *J. Power Sources*, 2019, **431**, 1–7.

2 Z. Wei, Z. Zhang, S. Chen, Z. Wang, X. Yao, Y. Deng and X. Xu, *Energy Storage Mater.*, 2019, **22**, 337–345.

3 X. Yang, M. Jiang, X. Gao, D. Bao, Q. Sun, N. Holmes, H. Duan, S. Mukherjee, K. Adair, C. Zhao, J. Liang, W. Li, J. Li, Y. Liu, H. Huang, L. Zhang, S. Lu, Q. Lu, R. Li, C. V. Singh and X. Sun, *Energy Environ. Sci.*, 2020, **13**, 1318–1325.

4 J. Wan, J. Xie, X. Kong, Z. Liu, K. Liu, F. Shi, A. Pei, H. Chen, W. Chen, J. Chen, X. Zhang, L. Zong, J. Wang, L.-Q. Chen, J. Qin and Y. Cui, *Nat. Nanotechnol.*, 2019, **14**, 705–711.

5 J. Wu, Z. Rao, Z. Cheng, L. Yuan, Z. Li and Y. Huang, *Adv. Energy Mater.*, 2019, **9**, 1902767.

6 H. Yuan, J. Luan, Z. Yang, J. Zhang, Y. Wu, Z. Lu and H. Liu, *ACS Appl. Mater. Interfaces*, 2020, **12**, 7249–7256.

7 T. Liu, J. Zheng, H. Hu, O. Sheng, Z. Ju, G. Lu, Y. Liu, J. Nai, Y. Wang, W. Zhang and X. Tao, *J. Energy Chem.*, 2021, **55**, 272–278.

8 Z. Lei, J. Shen, J. Wang, Q. Qiu, G. Zhang, S.-S. Chi, H. Xu, S. Li, W. Zhang, Y. Zhao, Y. Deng and C. Wang, *Chem. Eng. J.*, 2021, **412**, 128733.

9 R. Lei, Y. Yang, C. Yu, Y. Xu, Y. Li and J. Li, *Sustain. Energy Fuels*, 2021, **5**, 1538–1547.

10 H. Jamal, F. Khan, S. Hyun, S. W. Min and J. H. Kim, *J. Mater. Chem. A*, 2021, **9**, 4126–4137.

11 Z. Yang, Z. Sun, C. Liu, Y. Li, G. Zhou, S. Zuo, J. Wang and W. Wu, *J. Power Sources*, 2021, **484**, 229287.

12 Z. Lei, J. Shen, W. Zhang, Q. Wang, J. Wang, Y. Deng and C. Wang, *Nano Res.*, 2020, **13**, 2259–2267.

13 Y. Li, L. Zhang, Z. Sun, G. Gao, S. Lu, M. Zhu, Y. Zhang, Z. Jia, C. Xiao, H. Bu, K. Xi and S. Ding, *J. Mater. Chem. A*, 2020, **8**, 9579–9589.